Mixed-Valence Cyanopyridine-Bridged Complexes of Pentacyanoferrate and Pentaammineruthenium: Electronic Structure, Stability, and Redox Reactivity

Alejandra E. Almaraz,[†] Luis A. Gentil,[†] Luis M. Baraldo,*[,‡] and José A. Olabe*[,‡]

Departamento de Química, Facultad de Ciencias Exactas y Naturales, and Departamento de Ingeniería Química, Facultad de Ingeniería, Universidad Nacional de Mar del Plata, Mar del Plata 7600, Republic of Argentina, and Departamento de Química Inorgánica, Analítica y Química Física (INQUIMAE), Facultad de Ciencias Exactas y Naturales, Universidad de Buenos Aires, Pabellón 2, Ciudad Universitaria, Capital Federal 1428, Republic of Argentina

Received May 8, 1996[⊗]

The mixed-valence binuclear complexes, $[(NC)_5Fe(pyCN)Ru(NH_3)_5]^n$ (4- and 3-cyanopyridine isomers, with nitrile-*N* and pyridine-*N* binding to Ru and Fe, respectively) were prepared as solid compounds through stoichiometric oxidation of the fully reduced (II,II) binuclear complexes, R, with peroxydisulfate. By analysis of IR spectra, the solids were observed to be a mixture of the predominant electronic isomers with a Fe^{II}, Ru^{III} distribution, with minor amounts of the Fe^{III}, Ru^{II} isomers. In aqueous solution, R was oxidized with peroxydisulfate to M, the mixed-valence complex, and to Ox, the fully oxidized complex. The M complex shows an intervalence band at 938 nm; by application of the Hush model, it is described as a valence-trapped Ru^{II}, Fe^{III} complex; the latter electronic distribution is supported by UV−visible, electrochemical, and kinetic data, but a minor amount of the isomer with a Fe^{II}, Ru^{III} distribution is also present in the equilibrium. The M complex is unstable toward dissociation and further outer-sphere reactions, leading to hydrolyzed products in the time scale of minutes. Hydrolysis is also the main decomposition route of the Ox complex. In the reactions with excess peroxydisulfate, the analysis of successive spectra allows the elucidation of the rate constants for the one-electron processes leading to M and Ox. The rate constants for the formation and dissociation of M, as well as for the hydrolysis of Ox, were also obtained. A kinetic control is operative in the oxidation reactions, with a preferential attack of peroxydisulfate on the more reactive Ru(II) center. The role of electronic isomerization is discussed in the overall kinetic scheme, and the rate constant values for oxidation agree with predictions based on Marcus LFER, in accord with data published for related complexes.

Introduction

Interest in binuclear compounds containing $[Ru(NH_3)_5]^{2,3+}$ or $[Fe(CN)_5]^{2,3-}$,[1] led to a study of the kinetics of formation, dissociation, and redox reactions of the mixed-valence complex $[(NC)_5Fe(L)Ru(NH_3)_5]^n$ with L = pyrazine (pz).[2] An attempt to extend the work to L = cyanopyridine (CNpy) bridged complexes (hereafter, pyCN when the ligand binds through the pyridine nitrogen and NCpy when it binds through the nitrile group) was unsuccessful because of hydrolysis of NCpy when linked to the Ru(III) center, thus leading to deprotonated pyridinecarboxamido-bridged complexes.[3]

The homobinuclear bis(pentaammineruthenium) complexes with 4- and 3-CNpy have been studied,[4] and other CNpy-bridged complexes have been reported containing Ru(II) polypyridine moieties at one site and either $[Ru(NH_3)_5]^{3+}$ or $[Fe(CN)_5]^{2-}$ at the other site.[5] Bridging cyanopyridines have been used in intramolecular electron- and energy-transfer studies,[6,7] as well as in solvent-induced redox isomerization processes in binuclear asymmetric complexes.[8]

At the time of publication of Yeh's work,[3] we had preliminary albeit conclusive evidence that CNpy-bridged mixed-valence species of the pentacyanoferrate−L−pentaammineruthenium series could be characterized. We report herein spectroscopic and reactivity studies of the mixed-valence complexes with 4- and 3-CNpy (named hereafter as M_4 and M_3, respectively). The complexes were characterized as transient species in solution by oxidation of the fully reduced complexes (R_4, R_3). The R and M complexes were also obtained in the solid state. The oxidation reactions of these types of binuclear complexes with peroxydisulfate are of current mechanistic significance.[9]

Experimental Section

Materials. The following complexes were prepared as described in the literature: $[Ru(NH_3)_5L](PF_6)_2$ (L = 4- and 3-NCpy);[4,5a,10] sodium amminepentacyanoferrate(III) monohydrate;[11] sodium 4- and 3-(cyanopyridine)pentacyanoferrate(II) monohydrates;[12] *N*-methylpyrazinium iodide;[13] sodium amminepentacyanoferrate(II) trihydrate,[14] which was purified as described previously.[15] 4-Cyanopyridine and 3-cyanopyr-

[†] Universidad Nacional de Mar del Plata.
[‡] Universidad de Buenos Aires.
[⊗] Abstract published in *Advance ACS Abstracts,* November 15, 1996.

(1) Creutz, C. *Prog. Inorg. Chem.* **1983**, *30*, 1.
(2) Yeh, A.; Haim, A. *J. Am. Chem. Soc.* **1985**, *107*, 369.
(3) Huang, H. Y.; Chen, W. J.; Hang, C. C.; Yeh, A. *Inorg. Chem.* **1991**, *30*, 1862.
(4) Richardson, D. E.; Taube, H. *J. Am. Chem. Soc.* **1983**, *105*, 40.
(5) (a) Katz, N. E.; Creutz, C.; Sutin, N. *Inorg. Chem.* **1988**, *27*, 1687. (b) Cutin, E. H.; Katz, N. E.; *Polyhedron* **1991**, *10*, 653. (c) Cutin, E. H.; Katz, N. E. *Polyhedron* **1987**, *6*, 159.
(6) Szecsy, A. P.; Haim, A. *J. Am. Chem. Soc.* **1982**, *104*, 3063.
(7) Moore, K. J.; Lee, L.; Figard, J. M.; Gelroth, J. A.; Stimson, A. J.; Wohlers, H. D.; Petersen, J. D. *J. Am. Chem. Soc.* **1983**, *105*, 2274.
(8) Curtis, J. C.; Roberts, J. A.; Blackbourn, R. L.; Dong, Y.; Massum, M.; Johnson, C. S.; Hupp, J. T. *Inorg. Chem.* **1991**, *30*, 3856.
(9) Haim, A. *Taube Insights: From Electron Transfer Reactions to Modern Inorganic Chemistry*; Advances in Chemistry Series; American Chemical Society: in press.
(10) Clarke, R. E.; Ford, P. C. *Inorg. Chem.* **1970**, *9*, 495.
(11) Brauer, G. *Química Inorgánica Preparativa*, Reverté, S. A., Ed.; Barcelona, Buenos Aires, Mexico, 1958; p 909.
(12) Szecsy, A. P.; Miller, S. S.; Haim, A. *Inorg. Chim. Acta* **1978**, *28*, 189.
(13) Bahner, C. T.; Norton, L. L. *J. Am. Chem. Soc.* **1950**, *72*, 2881.
(14) Kenney, D. J.; Flynn, T. P.; Gallini, J. B. *J. Inorg. Nucl. Chem.* **1961**, *20*, 75.
(15) Jwo, J.; Haim, A. *J. Am. Chem. Soc.* **1976**, *98*, 1172.

S0020-1669(96)00489-2 CCC: $12.00

idine (Aldrich) were recrystallized from ethanol. Potassium peroxydisulfate (AnalaR) was recrystallized from hot water. Dimethyl sulfoxide (DMSO) and 4-acetylpyridine (Acpy) were used as received (Aldrich). All other chemicals for buffering and ionic strength maintenance were high-purity grade.

Synthesis of Complexes. The fully reduced complexes, Na-$[(NC)_5Fe(pyCN)Ru(NH_3)_5]\cdot nH_2O$, were prepared by dissolution of 0.06 mol of $[Ru(NH_3)_5(NCpy)](PF_6)_2$ in 5 mL of water, under argon. After the addition of an equimolar solution of $Na_3[Fe(CN)_5NH_3]\cdot 3H_2O$, the mixture was left for 30 min and was cooled in an ice bath. The solid was filtered off, washed with cold ethanol and ether, and dried over silica gel. Anal. Calcd for $Na[(NC)_5Fe(4pyCN)Ru(NH_3)_5]\cdot 5H_2O$: Fe, 9.5; Na, 3.9; Ru, 17.0; H_2O, 15.5; NH_3, 13.9. Found: Fe, 9.5; Na, 3.9; Ru, 17.2; H_2O, 15.3; 1 NH_3, 14.4. Calcd. for $Na[(NC)_5Fe(3pyCN)Ru(NH_3)_5]\cdot H_2O$: Fe, 10.8; Na, 4.4; Ru, 19.6; H_2O, 3.5; NH_3, 16.4. Found: Fe, 11.0; Na, 4.4; Ru, 19.0; H_2O, 3.4; NH_3, 15.9. The mixed-valence complexes, $[(NC)_5Fe(pyCN)Ru(NH_3)_5]\cdot 2H_2O$, were prepared by two different procedures: in the first one, 0.06 mol of the fully reduced complexes (with 4- or 3-CNpy) in 10 mL of water was oxidized with 0.03 mol of peroxydisulfate. While the mixture cooled at 0 °C, the precipitates formed immediately. The solids were filtered off, washed, dried, and stored under vacuum. In the second procedure, 0.06 mol of aquated $[Fe(CN)_5NH_3]^{3-}$ and freshly generated, equimolar $[Ru(NH_3)_5(NCpy)]^{3+}$ (obtained by mixing $[Ru(NH_3)_5(NCpy)]^{2+}$ with 0.03 mol of peroxydisulfate) was mixed in 10 mL of water, under argon. The solids also formed immediately and were handled as before. Anal. Calcd for $[(NC)_5Fe(pyCN)Ru(NH_3)_5]\cdot H_2O$: Fe, 11.3; Ru, 20.5; H_2O, 3.6; NH_3, 17.2. Found for the 4-pyCN complex: Fe, 11.3; Ru, 20.3; H_2O, 3.7; NH_3, 16.9. Found for the 3-pyCN complex: Fe, 11.3; Ru, 20.5; H_2O, 3.6; NH_3, 17.0. In both of the solid complexes, some contamination from sodium was detected: 0.3% and 0.6% for the 4- and 3-pyCN complexes, respectively.

Preparation of Solutions. Solutions of the R complexes were prepared by mixing equimolar, deoxygenated solutions of $[Fe(CN)_5H_2O]^{3-}$ and $[Ru(NH_3)_5(NCpy)]^{2+}$, at pH 5.5 (ethylenediaminetetraacetic acid (edta)−sodium acetate, ca. 10^{-3} M), $I = 0.1$ M (NaCl). The solutions of $[Fe(CN)_5H_2O]^{3-}$ (1×10^{-4} M) were prepared by dissolving sodium amminepentacyanoferrate(II) trihydrate and were used within 5 min (complete aquation), thus minimizing thermal decomposition processes.[16] Solutions of the oxidized binuclear complexes, M and Ox, were prepared by mixing fresh solutions of R with a controlled amount (1−10 equiv) of a solution of peroxydisulfate. Solutions of $[Fe(CN)_5H_2O]^{2-}$ were prepared according to the literature.[17] $[Ru(NH_3)_5(NCpy)]^{3+}$ and $[Fe(CN)_5(pyCN)]^{2-}$ (4- and 3-CNpy isomers) were prepared in solution by oxidation of the corresponding Ru(II) and Fe(II) complexes with peroxydisulfate. Solutions of *N*-methylpyrazinium nitrate were obtained by treating the iodide salt with silver nitrate and filtering off the silver iodide precipitate. Deionized water was further distilled after addition of alkaline potassium permanganate.

Analytical Methods. Sodium was determined by emission techniques, with a Shimadzu AA-640 spectrometer. Ruthenium and iron were determined by measuring spectrophotometrically the absorbances of ruthenium−thiocyanate and iron−phenantroline complexes, respectively.[18a] Water was determined by thermogravimetry, by heating the solids up to constant weight at 120 °C. For the analysis of ammonia, the solid complexes were treated with hot sulfuric acid; then the samples were neutralized with sodium hydroxide and distilled under boric acid; the resulting ammonium salt was titrated with a normalized solution of hydrochloric acid.[18b]

Ultraviolet, visible, and near-IR spectra were measured with the Shimadzu 210A and 260A spectrophotometers, or in a Hewlett-Packard 8452A diode-array instrument, interfaced with a rapid-mixing stopped-flow device (Applied Photophysics, Model RX 1000). The infrared spectra were recorded on a Perkin Elmer 599 spectrophotometer in KBr pellets.

Electrochemical Measurements. A LYP-M5 potentiostat, coupled with a PAR function generator and a Hewlett-Packard *X*−*Y* recorder Model 7004B were employed for cyclic voltammetry. A homemade three-electrode cell was used, with platinum wires as working and counter electrodes and a saturated calomel electrode as a reference. The solutions of the R complexes were handled in anaerobic conditions at 25 °C, pH = 5.5, $I = 0.1$ M (NaCl). The electroactive species were about $1-3 \times 10^{-4}$ M. Complementary measurements were made at pH 1.0.

Kinetic Measurements. The rate of formation of the binuclear complex $[(NC)_5Fe(4pyCN)Ru(NH_3)_5]^-$ (R_4) was measured by mixing freshly prepared aquated solutions of $[Fe(CN)_5NH_3]^{3-}$ with an excess of $[Ru(NH_3)_5(4NCpy)]^{2+}$, in a Hytech PQ-SF 53 stopped-flow instrument interfaced with a PC. The measurements were carried out by following the absorbance increase at 480 nm, near the maximum of the binuclear complex. For the 3-pyCN bridged dimer, R_3, the absorbance bands were too close to the bands of the reactants. By using a competitive technique with Acpy as a ligand, the formation reaction could be studied at 490 nm, by following the absorbance increase of the $[Fe(CN)_5(Acpy)]^{3-}$ ion,[19] as described elsewhere.[20] Rates of dissociation of the binuclear R complexes were measured by adding a 0.1 M solution of a scavenger ligand, either DMSO or $Mepz^+$ to a solution of the reactant, and following the decrease at the maximum wavelength of the binuclear complexes. In the experiment with $Mepz^+$, the increase at the absorption maximum of the product, $[Fe(CN)_5(Mepz)]^{2-}$, was also measured.[21] The measurements were carried out at 25 °C and $I = 0.1$ M (NaCl). Observed rate constants were calculated by least-squares fitting of the corresponding logarithmic traces.

Rates of oxidation of $[Ru(NH_3)_5L]^{2+}$ complexes (L = 4- and 3-NCpy) were measured by mixing solutions of the corresponding Ru(II) species (ca. 5×10^{-5} M) with an excess of peroxydisulfate ($(5-10) \times 10^{-4}$ M) and following the decay of the MLCT absorption of the reactant in stopped-flow conditions. Rates of oxidation of $[Fe(CN)_5(pyCN)]^{3-}$ were measured similarly in a conventional spectrophotometer.

In the reactions of the R complexes with peroxydisulfate, the solutions were mixed in a rapid-mixing device and the spectral evolution was recorded in the diode array instrument. In some experiments, an excess of $Mepz^+$ nitrate (0.1 M) was added to the solution of peroxydisulfate before mixing with the solutions of the R complexes. The reaction between $[Ru(NH_3)_5(4NCpy)]^{2+}$ and $[Fe(CN)_5H_2O]^{2-}$ complexes was studied using the same experimental arrangement.

Global Kinetic Analysis. The kinetic analysis of the data was performed using the Specfit software package, provided by Dr. Robert A. Binstead of Spectrum Software Associates, Chapel Hill, NC. Specfit is a global least-squares fitting routine for equilibrium and kinetic studies, which uses factor analysis decomposition methods. The factorized data can be fitted using a complex kinetic scheme (up to 14 equations). The solution of the differential equations system is achieved using a numerical integration (Bulirsch Stoer). The fit is improved by using a Marquardt iteration procedure. We estimated the errors in the constants as the dispersion in the values obtained from the fitting of several experiments. The errors are larger than the usual ones due to the covariance between the calculated spectra and the kinetic constants. The program is based on the published works of Zuberbühler et al.[22] A more detailed description of the use of the global analysis methodology has been recently published.[23] See also the Appendix (in the Supporting Information (SI).

Results

UV−vis−Near-IR Spectra of the R, M, and Ox Binuclear Complexes. Parts a and b of Figure 1 show the spectra of the

(16) Olabe, J. A.; Zerga, H. O. *Inorg. Chem.* **1983**, *22*, 4156.
(17) Macartney, D. H.; McAuley, A. *Can. J. Chem.* **1981**, *59*, 132.
(18) (a) Sandell, E. B. "*Chemical Analysis. Colorimetric Determination of Traces of Metals*; Interscience: New York, 1944; Vol. III, pp 271 and 391. (b) Kolthoff, I. M.; Sandell, E. B.; Meehan, E. J.; Bruckenstein, S. *Análisis Químico Cuantitativo*, 6th ed.; Nigar, S. R. L., Ed.; Buenos Aires, 1972; p 819.
(19) Murakami Iha, N. Y.; Toma, H. E. *An. Acad. Bras. Cienc.* **1982**, *54*, 491.
(20) Shepherd, R. E.; Taube, H. *Inorg. Chem.* **1973**, *12*, 1392.
(21) Toma, H. E.; Malin, J. M. *Inorg. Chem.* **1973**, *12*, 1039, 2080.
(22) (a) Gampp, H.; Maeder, M.; Meyer, C. J. Zuberbühler, A. D. *Talanta* **1985**, *32*, 95. (b) Gampp, H.; Maeder, M.; Meyer, C. J.; Zuberbühler, A. D. *Talanta* **1985**, *32*, 257. (c) Maeder, M.; Zuberbühler, A. D. *Anal. Chem.* **1990**, *62*, 2220.
(23) (a) Binstead, R. A.; Stultz, L. K.; Meyer, T. J. *Inorg. Chem.* **1995**, *34*, 546. (b) Stultz, L. K.; Binstead, R. A.; Reynolds, M. S.; Meyer, T. J. *J. Am. Chem. Soc.* **1995**, *117*, 2520.

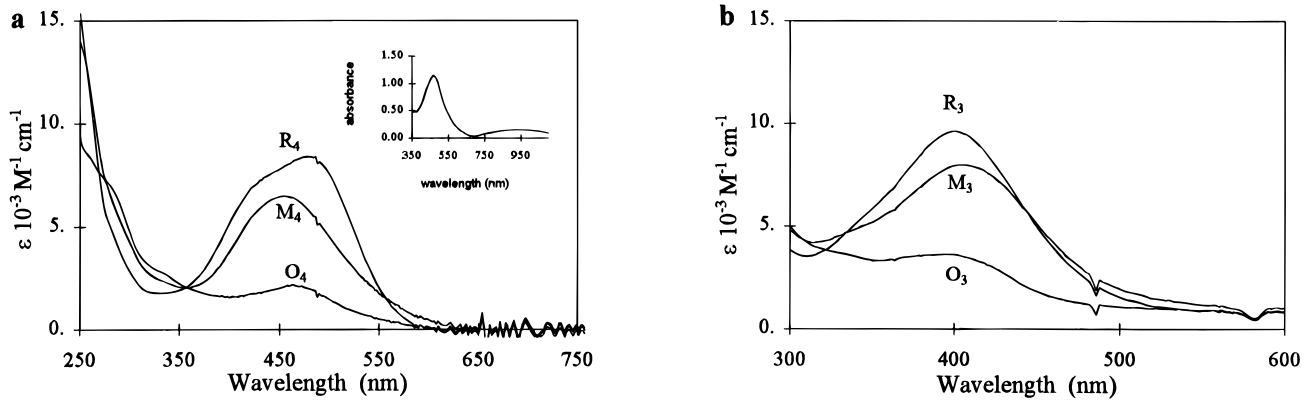

Figure 1. (a) Electronic spectra for the $[(NC)_5Fe^{II}(4pyCN)Ru^{II}(NH_3)_5]^-$ (R_4), $[(NC)_5Fe^{III}(4pyCN)Ru^{II}(NH_3)_5]^+$ (M_4), and $[(NC)_5Fe^{III}(4pyCN)Ru^{III}(NH_3)_5]^+$ (Ox_4), as calculated from the global analysis of the kinetic traces. (b) The same as above, but for $[(NC)_5Fe^{II}(3pyCN)Ru^{II}(NH_3)_5]^-$ (R_3), $[(NC)_5Fe^{III}(3pyCN)Ru^{II}(NH_3)_5]^+$ (M_3), and $[(NC)_5Fe^{III}(3pyCN)Ru^{III}(NH_3)_5]^+$ (Ox_3). (The inset shows the transient spectrum of M_4, in the reaction of R_4 with excess of peroxydisulfate.)

Table 1. Absortion Spectral Data, IR Wavenumbers, and Redox Potentials for Iron(II,III) and Ruthenium(II,III) Mononuclear and Binuclear Complexes

complex	λ_{max}, nm	$10^{-3}\epsilon_{max}$, M^{-1} cm^{-1}	ν_{NC}, cm^{-1}	ν_{CN}, cm^{-1}	δ_{NH_3}, cm^{-1}	E^0, V (NHE)
$[(NC)_5Fe^{II}(4pyCN)]^{3-}$	477	5.7	2242[b]	2050		0.54 (0.53[c])
$[(NC)_5Fe^{II}(3pyCN)]^{3-}$	414	3.2	2254[b]	2040		0.53 (053[c])
$[(NH_3)_5Ru^{II}(4pyCN)]^{2+}$	425	5.4 (10.2[c])	2179[d]		1260	0.62 (0.59[c])
$[(NH_3)_5Ru^{II}(3pyCN)]^{2+}$	401	5.6 (9.6[c])	2181[d]		1269	0.56 (0.56[c])
$[(NC)_5Fe^{III}(4pyCN)]^{2-}$	420	0.3				
	390	1.0				
$[(NC)_5Fe^{III}(3pyCN)]^{2-}$	410	1.0				
	362	1.0				
$[(NH_3)_5Ru^{III}(4pyCN)]^{3+}$	395	1.3				
	340 sh	1.2				
	258	4.0				
$[(NH_3)_5Ru^{III}(3pyCN)]^{3+}$	390	2.2				
	340 sh	2.2				
	250	6.7				
$[(NC)_5Fe^{II}(4pyCN)Ru^{II}(NH_3)_5]^-$	480	7.0 (15.9[c])	2190	2050	1280	0.5[e] (0.51[c])
	418	3.6 (sh[c])				
$[(NC)_5Fe^{II}(3pyCN)Ru^{II}(NH_3)_5]^-$	401	9.5	2186	2045	1287	0.52[e]
	350	sh				
$[(NC)_5Fe^{II,III}(4pyCN)Ru^{II,III}(NH_3)_5]$[f]	460	7.0	2240	2060	1310	0.66[g] (0.62[c])
	938	0.85	2175 sh	2115 sh	1270 sh	
$[(NC)_5Fe^{II,III}(3pyCN)Ru^{II,III}(NH_3)_5]$[f]	405	8.0	2210	2050	1305	0.60[g]
	700	sh	2185 sh	2110 sh	1285 sh	
$[(NC)_5Fe^{III}(4pyCN)Ru^{III}(NH_3)_5]^+$	460[h]	4.2				
	430[i]	4.0				
	280[h]	10.0				
$[(NC)_5Fe^{III}$-3pyCN-$Ru^{III}(NH_3)_5]^+$	395[h]	3.6				

[a] Reference 6. [b] Reference 5c. [c] Reference 3. [d] Reference 10. [e] Corresponds to the $Fe^{II,III}$ couple. [f] Predominantly Fe^{III}, Ru^{II} in solution and $Fe^{II,III}$ in the solid; see text. [g] Corresponds to the $Ru^{II,III}$ couple. [h] LMCT to Fe(III). [i] LMCT to Ru(III).

R_4, M_4, and Ox_4 and of the R_3, M_3, and Ox_3 complexes, respectively, in the visible region. The spectra of the M and Ox complexes result from the kinetic analysis of the successive spectra obtained in the reaction of the R complexes with excess of peroxydisulfate. The inset in Figure 1 shows a complete spectrum of M_4 measured at the time of maximum absorbance in the near-IR region. Band maxima, assignments and absorption coefficients are displayed in Table 1, together with data for the mononuclear complexes. The spectrum of M_4 was also measured at pH 1.0; the band at 460 nm remained unchanged, in contrast with the near-IR absorption, which shifted to lower energy.

IR Spectral Results of Solid Samples Containing the R and M Complexes. Solid samples containing the M complexes (4- or 3-CNpy) showed the same IR spectra, independently of the preparation method. Table 1 shows the relevant absorptions in the 2000−2300 cm^{-1} region (cyanide and nitrile stretchings), as well as in the 1300 cm^{-1} region (rocking deformations of coordinated ammines). Weak bands corresponding to other CNpy absorptions are omitted. Table 1 also includes the results obtained with the sodium salts of the fully reduced dimers, R_4 and R_3.

Electrochemistry. Figure SI 1 shows the cyclic voltammograms obtained for the 4- and 3-CNpy-bridged complexes at pH 5.5. For the 4-CNpy complex, two overlapping waves are clearly defined; each of them presents a difference of 60 mV between the anodic and cathodic peaks. For the 3-CNpy complex, only a broad wave is observed (peak separation ca. 130 mV), probably due to a strong overlap of two redox processes (Table 1). At pH 1.0, the $E_{1/2}$ of the first wave (E_1) was shifted to higher values, while the second value of $E_{1/2}$ (E_2) remained unchanged.

Formation and Dissociation Reactions of the R and M Complexes. The following rate law describes the rate of formation of the R_4 complex: $-d[[Fe(CN)_5H_2O]^{3-}]/dt = d[R_4]/dt = k_{obs}[[Fe(CN)_5H_2O]^{3-}]$. From the linear plot of k_{obs} against the concentration of $[[Ru(NH_3)_5(4NCpy)]^{2+}]$, a value of $k_{f(4NCpy)} = (1.6 \pm 0.1) \times 10^3$ M^{-1} s^{-1} was obtained from the slope. For

Table 2. Elementary Steps Involved in the Reaction of R with Peroxydisulfate

eq	reaction[a]	$k_{forward}$[b]	$k_{reverse}$[b]
1	$[Fe^{II}(pyCN)Ru^{II}]^- \rightleftharpoons [Fe^{II}H_2O]^{3-} + [Ru^{II}(NCpy)]^{2+}$	$(2.4 \pm 0.1) \times 10^{-3}$ ($(3.9 \pm 0.1) \times 10^{-3}$)	$(1.6 \pm 0.1) \times 10^{3}$ ($(1.9 \pm 0.1) \times 10^{3}$)
2	$[Fe^{III}(pyCN)Ru^{II}] \rightleftharpoons [Fe^{II}(pyCN)Ru^{III}]$		
3	$[Fe^{II}(pyCN)Ru^{III}] \rightleftharpoons [Fe^{II}H_2O]^{3-} + [Ru^{III}(NCpy)]^{3+}$	$(8 \pm 3) \times 10^{-3}$ ($(10 \pm 4) \times 10^{-3}$)[c,d]	$(3 \pm 1) \times 10^{3}$ ($(3 \pm 1) \times 10^{3}$)[c]
4	$[Fe^{II}H_2O]^{3-} + [Ru^{III}(NCpy)]^{3+} \rightleftharpoons [Fe^{III}H_2O]^{2-} + [Ru^{II}(NCpy)]^{2+}$	$>5 \times 10^{6}$ ($>1 \times 10^{6}$)[e]	$<5 \times 10^{4}$ ($<1 \times 10^{4}$)[e]
5	$[Fe^{II}H_2O]^{3-} + [Mepz]^{+} \rightleftharpoons [Fe^{II}Mepz]^{2-}$	$(2.4 \pm 0.1) \times 10^{3}$ [f]	$(2.8 \pm 0.1) \times 10^{-4}$ [f]
6	$[Ru^{III}(NCpy)]^{3+} + H_2O \rightarrow [Ru^{III}(NHC(O)py)]^{2+} + H^+$	$(2.85 \pm 0.02) \times 10^{-3}$ ($(4.39 \pm 0.02) \times 10^{-3}$)[g]	
7	$[Fe^{II}(pyCN)Ru^{II}]^- + [Fe^{III}(pyCN)Ru^{III}]^{+} \rightleftharpoons 2\,[Fe^{II}(pyCN)Ru^{III}]$	$2 \pm 1 \times 10^{6}$ ($(0.5 \pm 0.1) \times 10^{6}$)[c]	
8	$[Fe^{III}(4pyCN)Ru^{II}] + [S_2O_8]^{2-} \rightarrow [Fe^{III}(4pyCN)Ru^{III}]^{+} + [SO_4]^{2-} + [SO_4]^{\bullet-}$	$3.7 \pm 0.4 \times 10^{2}$ ($(6.3 \pm 0.6) \times 10^{2}$)[c]	
9	$[Fe^{III}(pyCN)Ru^{III}]^{+} + H_2O \rightarrow [Ru^{III}(NHC(O)py)Fe^{III}]^{-} + H^+$	$2 \pm 1 \times 10^{-2}$ ($<0.5 \times 10^{-2}$)[c]	
10	$[Fe^{II}(4pyCN)Ru^{II}]^- + [S_2O_8]^{2-} \rightarrow [Fe^{II}(4pyCN)Ru^{III}] + [SO_4]^{2-} + [SO_4]^{\bullet-}$	$6.5 \pm 1.0 \times 10^{2}$ ($(6.0 \pm 0.4) \times 10^{2}$)[c]	
11	$[Ru^{II}(NCpy)]^{2+} + [S_2O_8]^{2-} \rightarrow [Ru^{III}(NCpy)]^{3+} + [SO_4]^{2-} + [SO_4]^{\bullet-}$	$2.0 \pm 0.1 \times 10^{3}$ ($(4.4 \pm 0.1) \times 10^{3}$)	
12	$[Fe^{II}(pyCN)]^{3-} + [S_2O_8]^{2-} \rightarrow [Fe^{III}(pyCN)]^{2-} + [SO_4]^{2-} + [SO_4]^{\bullet-}$	1.0 ± 0.5 (1.3 ± 0.5)	
13	$[Fe^{II}(pyC(O)NH)Ru^{III}]^- + H_2O \rightleftharpoons [Fe^{II}H_2O]^{3-} + [Ru^{III}(NHC(O)py)]^{2+}$	$2.56 \pm 0.05 \times 10^{-3}$ ($(2.75 \pm 0.05) \times 10^{-3}$)[g]	(2.52 ± 0.05) ($(3.41 \pm 0.05) \times 10^{3}$)[g]
14	$[Fe^{II}(4pyCN)Ru^{III}] + H_2O \rightarrow [Fe^{II}(4pyC(O)NH)Ru^{III}]^- + H^+$	$<1 \times 10^{-3}$ ($<1 \times 10^{-3}$)	

[a] In all cases, Fe and Ru describe the pentacyanoiron and pentaammineruthenium fragments, respectively. [b] The values correspond to the 4-CNpy complexes and, in parentheses, to the 3-CNpy complexes. Units are in s^{-1} for the dissociation and hydrolisis reactions and in $M^{-1}\ s^{-1}$ for the formation and redox reactions. [c] Calculated from the global kinetic analysis. The errors in these values were determined from the dispersion obtained in the fitting of several experiments. [d] The reported values are equal to k_{obs}/K_{et}. because the rapid preequilibrium of eq 2 was not considered in the kinetic analysis. [e] These constants have been initialy estimated form the Marcus cross-relation. In this table we inform a lower (or upper) limit to their values that does not affect the fitting. [f] Reference 21. [g] Reference 3.

the R_3 complex, under competitive conditions with Acpy, the rate law was $-d[[Fe(CN)_5H_2O]^{3-}]/dt = d[[Fe(CN)_5(Acpy)]^{3-}] = k_{obs}\,[[Fe(CN)_5H_2O]^{3-}]$, with $k_{obs} = k_{f(Acpy)}[Acpy] + k_{f(3NCpy)}[[Ru(NH_3)_5(3NCpy)]^{2+}]$. Similarly, $k_{f(3NCpy)} = (1.9 \pm 0.1) \times 10^3\ M^{-1}\ s^{-1}$ was obtained by plotting k_{obs} against the concentration of $[Ru(NH_3)_5(3NCpy)]^{2+}$.

In the dissociation of the R dimers, the rate law was $-d[R]/dt = k_{obs}[R]$ for the experiments with either DMSO or $Mepz^+$ as scavengers for the $[Fe(CN)_5H_2O]^{3-}$ product. For $Mepz^+$, the same rate law and k_{obs} value were obtained by measuring the rate of increase of absorption of $[Fe(CN)_5(Mepz)]^{2-}$. Under the saturation conditions, k_{obs} values can be associated to k_d, the specific dissociation rate constant of R. The values were $(2.4 \pm 0.1) \times 10^{-3}$ and $(3.9 \pm 0.1) \times 10^{-3}\ s^{-1}$ for the 4- and 3-CNpy-bridged complexes, respectively.

The formation reactions of the M complexes could not be studied by a similar direct method. A clean solution of M cannot be generated by mixing $[Ru(NH_3)_5(NCpy)]^{3+}$ with a solution of $[Fe(CN)_5H_2O]^{3-}$ because a rapid outer-sphere reaction leads to a mixture of predominantly Fe(III) (which is kinetically inert) and Ru(II). The formation and dissociation rate constants of M can be obtained through the kinetic analysis of the reaction of R with peroxydisulfate, as shown below (see Table 2 and Appendix, SI).

Reactions of the R Complexes with 1 equiv of Peroxydisulfate. Parts a−c of Figure SI 2 show the successive spectra obtained in the experiment with R_4 for increasing time periods after the mixing of reactants. In Figure SI 2a (0−90 s), it can be seen that the asymmetric band of R_4 decays and transforms into a single band centered at 460 nm, with isosbestic points at 355 and 556 nm. The absorbance increase in the low-energy region corresponds to the onset of a new band centered at 938 nm (Figure 1, inset). In Figure SI 2b (90−600 s), the 460 nm band (and also the 938 nm band, not seen in the figure) decay simultaneously, leading to a band centered at 425 nm, with an isosbestic point at the same wavelength and a shoulder at 480 nm. For longer times, Figure SI 2c shows that the absorptions at 425 and 480 nm slowly decrease and increase, respectively, with an isosbestic point at 465 nm. Figure SI 2d shows a complementary experiment: by mixing equimolar solutions of $[Ru^{II}(NH_3)_5(4NCpy)]^{2+}$ and $[Fe^{III}(CN)_5H_2O]^{2-}$, the changes are similar to those described in Figure SI 2c.

Parts a−c of Figure SI 3 show the corresponding successive spectra for R_4, with initial addition of $Mepz^+$. Behavior similar to that in Figure SI 2 is observed in the 350−550 nm region for the three time scales. In Figure SI 3c, however, not only an absorbance decrease at 425 nm but a shift of the maximum to lower wavelengths is observed. The new feature in Figure SI 3 is the onset of a band at 665 nm, with an isosbestic point at 560 nm.

Parts a and b of Figure SI 4 show the results with R_3. In Figure SI 4a, the initial changes show a decrease of absorption at 400 nm and an increase in the UV region, with an isosbestic point at 325 nm. Figure SI 4b shows the subsequent changes in a slower time scale; a shift to lower wavelengths with an increase in intensity and a new isosbestic point at 400 nm are observed. No additional changes were detected in the spectra for longer time scales, as was the case with R_4 (Figure SI 2c).

Spectral and Kinetic Results for the Oxidation of Mononuclear and Binuclear (R_4 and R_3) Species with Excess Peroxydisulfate. (i) Oxidation of $[Ru(NH_3)_5(NCpy)]^{2+}$. The spectra of the products of the reactions of $[Ru(NH_3)_5(NCpy)]^{2+}$ (4- and 3-isomers) with peroxydisulfate can be assigned to the $[Ru(NH_3)_5(NCpy)]^{3+}$ species (Table 1). Good pseudo-first-order plots were obtained for the oxidation reactions of the mononuclear complexes of 4- and 3-NCpy. From the k_{obs} values, the values for the second-order rate constants were obtained as described before for the formation reactions (Table 2). The original MLCT bands characteristic of Ru(II) complexes are quantitatively recovered when the *freshly prepared* solutions

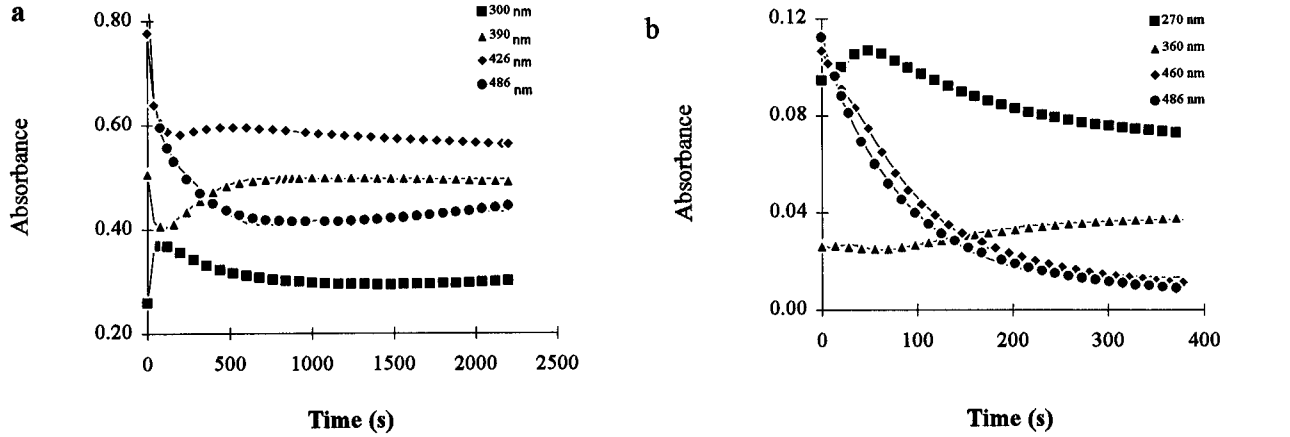

Figure 2. **(a)** Experimental (●) and fit (—) kinetic traces for the reaction of $[(NC)_5Fe^{II}(4pyCN)Ru^{II}(NH_3)_5]^-$ with 1 equiv of peroxydisulfate, according to the model proposed in Scheme 1. (b) The same as above, but for the reaction of $[(NC)_5Fe^{II}(4pyCN)Ru^{II}(NH_3)_5]^-$ with excess of peroxydisulfate.

of the Ru(III) complexes were reduced with either Cr(II) or ascorbic acid. On the other hand, aged Ru(III) solutions show an increase in absorption at 390 nm, associated to hydrolytic processes in a longer time scale, without recovery of the MLCT absorption upon reduction.

(ii) Oxidation of $[Fe(CN)_5(pyCN)]^{3-}$. By oxidation with peroxydisulfate, the MLCT bands typical of the Fe(II) complexes disappear. The spectra of the products (which remain unchanged for hours) can be assigned to the corresponding Fe(III) complexes (Table 1). The reduced Fe(II) species are quantitatively recovered by treating with ascorbic acid. In the oxidation reaction, the fits of $\ln [A_\infty - A_t]$ *vs t* were linear only for a half-life. Similar deviations of the fits have been observed previously with the pz complex.[2] By plotting k_{obs} against the concentration of peroxydisulfate, a linear plot is obtained with a nonzero intercept: $k_{obs} = k_a + k_b [S_2O_8^{2-}]$, with $k_a = (1.0 \pm 0.3) \times 10^{-3}$ s^{-1} and $k_b = 1.0 \pm 0.5$ M^{-1} s^{-1}. The rate law can be interpreted as arising from the competition of the dissociation and oxidation reactions. The value of k_a is consistent with the dissociation rate constant of the Fe(II) complexes; thus, the values of k_b can be assigned to the specific second-order rate constant for the oxidation processes (Table 2).

(iii) Oxidation of the R_4 and R_3 Complexes. Parts a−c of Figure SI 5 show the results for R_4. In Figure SI 5a (0−70 s), the changes are similar to those described in Figure 2a. A band centered at 938 nm also develops. In Figure SI 5b (70−154 s), an absorbance decrease is observed for the 400−600 and 250−300 nm regions, while an increase occurs for the 300−400 nm region, with isosbestic points at 300 and 390 nm. During this time period the absorption at 938 nm also decays. Finally, Figure SI 5c (154−378 s) shows the same absorbance trends as before (although slower), with the final onset of a broad absorption in the 320−400 nm region and a shoulder at 475 nm.

For the oxidation of the R_3 complex, Figure SI 6a shows the initial spectral changes after mixing; they are similar to those described in Figure SI 5a. The subsequent spectra (Figure SI 6b) show the onset of a band centered at 390 nm and a shoulder at 330 nm, with an isosbestic point at 320 nm. For longer times, much slower spectral changes (compared to those described in Figure SI 5c) were detected, with an increase and decrease of absorption at 380 and 270 nm, respectively, and an isosbestic point at 300 nm.

Discussion

Electronic Structure of the R, M, and Ox Complexes in Aqueous Solution. We assign the main peak of the asymmetric band centered at 480 nm in R_4 (Figure 1a) to a MLCT transition from Fe(II) to the π^* (pyCN) orbital, by comparison with the spectrum of $[Fe(CN)_5(4pyCN)]^{3-}$ (Table 1). Thus, the shoulder at ca. 420 nm is traced to the MLCT transition from Ru(II) to the nitrile-antibonding orbital. We assign the peaks at 401 nm and the shoulder at 350 nm to the corresponding transitions in R_3 (Figure 1b).

The spectrum of M_4 suggests that it is the electronic isomer with a $[Fe^{III}, Ru^{II}]$ distribution. We assign the 460 nm band to a MLCT transition from $d\pi(Ru^{II})$ to π^*(NCpy), shifted to lower energy with respect to the corresponding transition in R_4 and in mononuclear $[Ru(NH_3)_5(4NCpy)]^{2+}$; this is as expected from the presence of a Lewis acid, $[Fe^{III}(CN)_5^{2-}]$. The alternative formulation as the electronic isomer with a $[Fe^{II}, Ru^{III}]$ distribution can be ruled out on the following basis: other binuclear complexes (e.g. with pz or 4,4′-bpy as bridging ligands, featuring a $[Fe^{II}, Ru^{III}]$ distribution) show the expected decrease in energy of the $d\pi(Fe^{II}) \rightarrow \pi^*$(L) transition when an electron withdrawing moiety binds to the exposed end of L;[2] this is not the case here. The $E°$ values of the mononuclear ions also suggest that the iron center is more easily oxidizable (Table 1). Finally, the constancy in the energy of the MLCT band at 460 nm at lower pH points to Ru(II) being the donor center (the protonation on cyanides should shift the $d\pi(Fe^{II}) \rightarrow \pi^*$(pyCN) transition toward higher energies).[21]

On the above basis, we assign the band at 938 nm (inset, Figure 1) to a MM′CT, $Ru^{II} \rightarrow Fe^{III}$ intervalence transition. The shift to lower energies at pH 1 is consistent with Fe(III) becoming a stronger acceptor as a result of cyanide protonation.[24]

After the 1 equiv oxidation of R_3, the product shows a band at 405 nm and a shoulder at ca. 335 nm (Figure 1b). The shape of the band suggests that both MLCT transitions (from Fe(II) and from Ru(II) to the corresponding antibonding orbitals in the bridged ligand) are present. This could be indicative of the coexistence of significant amounts of both electronic isomers in equilibrium, containing the $[Fe^{II}, Ru^{III}]$ and the $[Fe^{III}, Ru^{II}]$ distributions, as also suggested by the electrochemical data discussed below. A very weak shoulder was found at ca. 700 nm, and we assign it tentatively to the intervalence transition(s) in $M_3(M'_3)$, by analogy with the assignments performed for the bis(pentaammineruthenium) ion.[4]

The spectra of the Ox complexes (Figure 1) are consistent with the data for the mononuclear complexes of Fe(III) and Ru(III). We assign the bands in the visible region (Table 1) to

(24) Macartney, D. H. *Inorg. Chem.* **1991**, *30*, 3337.

Table 3. Intervalence Band Maxima, Intensities, and Widths for Some Binuclear Complexes and Calculated Coupling and Delocalization Parameters (Hush Model)[a]

complex	λ_{max}, nm (kK)	$10^{-}\epsilon_{max}$, M^{-1} cm^{-1}	$\Delta\bar{\nu}_{1/2}$, kK (exp; calc)[b]	H_{ab}, cm^{-1}	10^3 α^2	ref
$[(NC)_5Fe^{III}(4pyCN)Ru^{II}(NH_3)_5]$	938 (10.7)	850	3.9; 4.9	410	1.5	this work
$[(NH_3)_5Ru^{III}(4pyCN)Ru^{II}(NH_3)_5]^{5+}$	935 (10.7)	1100	5.2	535		4
$[(NC)_{5Fe}{}^{II}(pz)Ru^{III}(NH_3)_5]$	1650 (6.1)	1550	4.3; 3.7	600	9.8	2

[a] Measurements in aqueous solution. [b] From $\Delta\bar{\nu}_{1/2} = [2310(\nu_{max} - E_0)]^{1/2}$. [c] From $H_{ab} = 2.05 \times 10^{-2}\,[\epsilon_{max}\Delta\bar{\nu}^1{}_{/2}/\bar{\nu}_{max}]^{1/2}[\bar{\nu}_{max}/r]$ with $r = 9.3$ Å. [d] From $a = H_{ab}/\bar{\nu}_{max}$.

LMCT transitions from cyanides to the Fe(III) center.[25] LMCT transitions to the Ru(III) center are expected at higher energies.[26] We emphasize that the Ox complexes are unstable with respect to hydrolysis (see below).

Electrochemical Measurements. The results for the 4-CNpy binuclear complex (Table 1) can be associated with the following redox processes:

$$[(NC)_5Fe^{III}(4pyCN)Ru^{III}(NH_3)_5]^+ + e^- \rightarrow \underset{Ox_4}{}$$
$$\underset{M_4}{[(NC)_5Fe^{III}(4pyCN)Ru^{II}(NH_3)_5]} \qquad E_2(4) = 0.66\ V$$

$$[(NC)_5Fe^{III}(4pyCN)Ru^{II}(NH_3)_5] + e^- \rightarrow \underset{M_4}{}$$
$$\underset{R_4}{[(NC)_5Fe^{II}(4pyCN)Ru^{II}(NH_3)_5]^-} \qquad E_1(4) = 0.50\ V$$

$E_2(4)$ is similar to values found for the reduction of Ru(III) in binuclear complexes with neighboring electron-withdrawing M(III) centers.[2] $E_1(4)$ is slightly lower than the value found for the reduction of $[Fe(CN)_5(4pyCN)]^{2-}$, and this is in keeping with the π-donor influence of $[Ru(NH_3)_5{}^{2+}]$. Therefore, we confirm the M_4 dimer as having a $[Fe^{III}, Ru^{II}]$ distribution. The results at pH 1 support this assignment: while $E_2(4)$ remains unchanged, $E_1(4)$ is shifted to higher values, as expected from protonation of cyanides.[25]

In the 3-CNpy dimer, we infer, considering the broad shape of the wave, that the two reduction processes are also operative. The estimated $E_2(3)$ and $E_1(3)$ values are 0.60 and 0.53 V, respectively.

Intervalence Band. Application of Theoretical Models. The calculations based on the Hush model[27] were performed with data for the M_4 dimer (Table 3). The value for α^2 (a measure of the delocalization in the ground state) suggests the onset of valence-trapped centers. The value of the electronic coupling parameter, H_{FeRu}, is similar to those for other weakly coupled complexes, also displayed in Table 3. The higher energy and lower intensity of the IV band in M_3 compared to M_4 is in keeping with a weaker coupling in the first complex, as found in the bis(pentaammineruthenium) analogs.[4]

Electronic Structure of the R and M Complexes in the Solid Phase. The IR results with the R complexes (Table 1) are diagnostic of oxidation states II for both metal centers.[3] The values of ν(NC) are similar to those in the $[Ru(NH_3)_5(NCpy)]^{2+}$ species, showing a significant decrease with respect to the free ligand values (2240 and 2235 cm^{-1} for 4- and 3-CNpy, respectively); this is related to the strong $d\pi(Ru^{II}) \rightarrow \pi^*$(NC) back-donation. Similarly, the values of ν(CN) and $\delta(NH_3)$ are diagnostic of the cyanide and ammine ligands being coordinated to M(II) species.[28,29] In the M complexes, the pattern of strong and weak bands suggest that a mixture of the electronic isomers is present. From the wavenumbers of the most intense peaks, we infer that the $[Fe^{II}(pyCN)Ru^{III}]$ species are predominant. The values of ν(NC) are slightly lower than those measured for Ru(III)−nitrile mononuclear complexes (ca. 2270 cm^{-1}),[30] in agreement with some back-bonding influence of the pentacyanide moiety. The values of $\delta(NH_3)$ agree with the latter assignment. The intense peaks in the C−N stretching region at 2050−2060 cm^{-1} are diagnostic of Fe(II).

The weaker peaks for each of the mixed-valence complexes suggest that minor amounts of the electronic isomers with the $[Fe^{III}(pyCN)Ru^{II}]$ distribution are also present. The shoulders at ca. 2180 and 1280 cm^{-1} are indicative of Ru(II); however, this could also be traced to small impurities from the R complexes (cf. analytical results and, below, the decomposition scheme associated to M_4). The shoulders at 2110−2115 cm^{-1} are indicative of C−N stretchings arising in Fe(III) species.[31]

To confirm the above interpretation, we show the results obtained with the $[(NC)_5Ru^{II}(4pyCN)Ru^{III}(NH_3)_5]$ analog:[32] ν_{NC} = 2200 cm^{-1}; ν_{CN} = 2068 cm^{-1}; δ_{NH3} = 1300 cm^{-1}. Here, the oxidation states of the non-equivalent ruthenium centers are clearly defined, because the redox potentials of the $Ru^{III,II}$ couples are much more separated (1.15 and 0.55 V for the cyanide- and ammine-containing metal centers, respectively). Thus, the presence of only one stable isomer carrying the +3 charge at the nitrile-binding center is clearly demonstrated.[33]

The presence of different amounts of each of the electronic isomers in the solution and solid phases is an interesting example of the competition of different factors on their relative stabilities. While in aqueous solution the electronic effects associated with the strong Ru(II)−NC interaction seem to be predominant over the electrostatic effects otherwise favoring the unstable electronic isomer, it is probable that in a delicate equilibrium situation, as reported here, the electrostatic factors controlling the lattice energies are determinant for the predominant stabilization of the more highly charged species in the solid state, associated with the $[Fe^{II}, Ru^{III}]$ distribution.

Stability of the Binuclear R, M, and Ox Complexes in Aqueous Solution. We consider the possible reaction modes listed in Scheme 1. Instability factors can be traced to several processes: dissociation into the mononuclear species, hydrolytic reactions, disproportionation into the isovalent states or electronic isomerization reactions. We discuss the relevance of these reaction modes for the three binuclear complexes, R, M, and Ox.

(25) Johnson, C. R.; Henderson, W. W.; Shepherd, R. E. *Inorg. Chem.* **1984**, *23*, 2754.
(26) Chou, M. H.; Creutz, C.; Sutin, N. *Inorg. Chem.* **1992**, *31*, 2318.
(27) Hush, N. S. *Prog. Inorg. Chem.* **1967**, *8*, 391.
(28) Yeh, A.; Haim, A.; Tanner, M.; Ludi, A. *Inorg. Chim. Acta* **1979**, *33*, 51.
(29) Olabe, J. A.; Haim, A. *Inorg. Chem.* **1989**, *28*, 3277.
(30) Clarke, R. E.; Ford, P. C. *Inorg. Chem.* **1970**, *9*, 227.
(31) Sharpe, A. G. *The Chemistry of Cyano Complexes of the Transition Metals*; Academic Press: New York, 1976; Chapter VII.
(32) Almaraz, A. E.; Gentil, L. A.; Baraldo, L. M.; Olabe, J. A., Submitted for publication.
(33) Siddiqui, S.; Henderson, W. W.; Shepherd, R. E. *Inorg. Chem.* **1987**, *26*, 3101.

Scheme 1

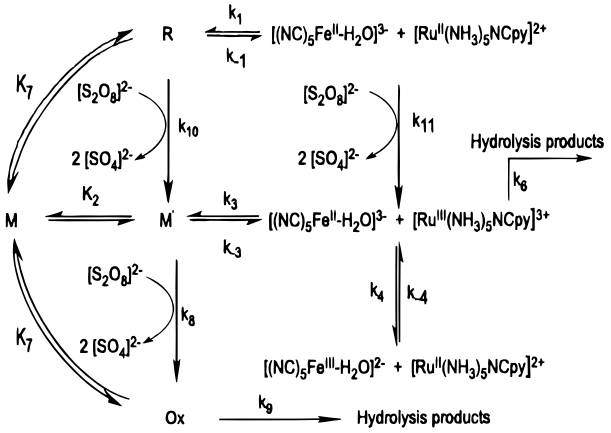

(i) R Complexes. The main source of unstability of the R complexes arises from reaction 1:

$$[(NC)_5Fe^{II}(pyCN)Ru^{II}(NH_3)_5]^- \leftrightarrow [Fe^{II}(CN)_5H_2O]^{3-} + [Ru^{II}(NH_3)_5(NCpy)]^{2+} \qquad k_{-1}, k_1 \quad (1)$$

The stability constants, $K_{st} = k_1/k_{-1}$ are 6.9×10^5 and 4.8×10^5 M^{-1}, for 4- and 3-CNpy, respectively. They are both of the same order as values obtained for other binuclear complexes of the same series with dipositively charged Ru(II) species.[2] The 4-CNpy complex is more stable than the 3-CNpy isomer, mainly because k_{-1} is lower, reflecting the stronger back-bonding in the first complex. The k_{-1} values are indicative of the cleavage of the Fe−N(py) bond but not the Ru−N(nitrile) bond; they are higher by a factor of 2 with respect to k_{-1} values in the corresponding $[Fe^{II}(CN)_5(pyCN)]^{3-}$; $[Ru^{II}(NH_3)_5L]^{2+}$ are much more inert toward dissociation of the L ligand than $[Fe(CN)_5L]^{3-}$, because of the stronger σ-donor and π-acceptor interactions in the Ru(II) complexes.[34] In contrast to k_{-1}, the k_1 values are very similar for the 4- and 3-CNpy isomers. They are both of the same order as values measured for the entry of other $[Ru^{II}(NH_3)_5L]^{2+}$ species into $[Fe(CN)_5H_2O]^{3-}$ (L = pz, bpy).[2] The values of k_{-1} and k_1 are indicative of a dissociative mechanism, typical of the behavior of $[Fe(CN)_5L]^{n-}$ complexes.[35]

An additional source of instability of the R complexes is given by the spontaneous thermal decomposition of $[Fe(CN)_5H_2O]^{3-}$,[16] which makes reaction 1 irreversible in the long time scale (hours); this is not relevant to our present study.

According to the value of K_{st} in reaction 1, significant (up to 5−10%) amounts of the mononuclear species can be present in the equilibrium mixtures obtained by handling solutions of R in the concentration range $(5-10) \times 10^{-5}$ M. This is relevant to the global analysis procedure, because the reactivity of the mononuclear species toward peroxydisulfate must be considered (see Appendix, SI).

(ii) M Complexes. In the reaction of R_4 with 1 equiv of peroxydisulfate, the successive spectra at the early stages (Figure SI 2a) show that M_4 is formed. However, the successive spectra for longer times (Figure SI 2b) show the decay of M_4, together with the appearance of $[Ru^{II}(NH_3)_5(4NCpy)]^{2+}$ (425 nm). From the kinetic analysis, the k_{obs} value associated with the decay of M_4 is ca. 10^{-3} s^{-1}. Although the product is consistent with the dissociation of M_4, the rate is anomalously high for the cleavage of a Fe^{III}−pyCN bond.[36] On the other hand, k_{obs} is consistent with the cleavage of a Fe^{II}−pyCN bond.[12] We propose that a rapid electronic isomerization process is operative:

$$[(NC)_5Fe^{III}(4pyCN)Ru^{II}(NH_3)_5] \leftrightarrow [(NC)_5Fe^{II}(4pyCN)Ru^{III}(NH_3)_5] \qquad K_{et4} \quad (2)$$

(M_4 ⇔ M'_4)

followed by a dissociation of the M'_4 complex into $[Fe^{II}(CN)_5H_2O]^{3-}$ and $[Ru^{III}(NH_3)_5(4NCpy)]^{3+}$ according to eq 3, with $k_{obs} = K_{et4}k_{-3}$.

$$[(NC)_5Fe^{II}(4pyCN)Ru^{III}(NH_3)_5] \leftrightarrow [Fe^{II}(CN)_5H_2O]^{3-} + [Ru^{III}(NH_3)_5(4NCpy)]^{3+} \qquad k_{-3}, k_3 \quad (3)$$

The formation of $[Ru^{II}(NH_3)_5(4NCpy)]^{2+}$ (Figure SI 2b) can be explained by a rapid equilibration:

$$[Fe^{II}(CN)_5H_2O]^{3-} + [Ru^{III}(NH_3)_5(4NCpy)]\ ]^{3+} \leftrightarrow [Fe^{III}(CN)_5H_2O]^{2-} + [Ru^{II}(NH_3)_5(4NCpy)]^{2+} \qquad k_4, k_{-4} \quad (4)$$

An initial value estimated for the rate constants of eq 4 was obtained by applying the Marcus cross-reaction, considering available data for the $E°$ and the estimated self-exchange rate constant values of the mononuclear redox couples, taking into account ion-pairing effects.[37] Evidently, the $[Fe(CN)_5H_2O]^{3-}$ ion reacts much faster according to eq 4 than to the reverse of eq 3. An independent check of the occurrence of reaction 4 was obtained by approaching the equilibrium through the mixing of the mononuclear Fe(III) and Ru(II) ions. In that case, the same spectra as those in Figure SI 2b were obtained. Moreover, the subsequent slow changes described in Figure SI 2c,d were also observed. The absorbance decrease at 425 nm, together with the increase at 480 nm, suggests that R_4 builds up according to the reverse of eq 1.

In order to obtain a value for k_{-3}, we need to estimate K_{et4} (eq 2). In view of the close values of $E_1(4)$ and $E_2(4)$, the possibility of a minor amount of the electronic isomer M'_4 being present in the equilibrium mixture of the mixed-valence species should be considered. From the following thermodynamic cycle

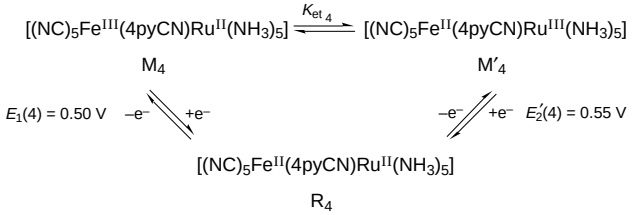

the equilibrium constant, K_{et4}, for the interconversion of electronic isomers, M_4 and M'_4, can be calculated. $E_1(4)$ is the measured potential for the first oxidation wave of R_4, 0.50 V, and $E_2'(4)$ is an estimated value, taken equal to the one measured in the "model" complex $[(NC)_5Ru^{II}(4pyCN)Ru^{II}(NH_3)_5]^-$, 0.55 V.[32] The latter number reflects the oxidation ability of the $[Ru^{II}(NH_3)_5(4NCpy)]^{2+}$ site when the neighboring metal center is in the oxidation state (II) (note that the $[Ru^{II}(CN)_5]^{3-}$ site is oxidized at a much higher potential, 1.15 V).[32] Accordingly, M_4 is stabilized over M'_4 by 0.05 V (1.2 kcal/mol) and thus $K_{et4} = 0.13$. Thus, the electrochemical results indicate that M_4 is the predominant electronic isomer, by about 90%.

(34) Taube, H. *Pure Appl. Chem.* **1979**, *51*, 901.
(35) Macartney, D. H. *Rev. Inorg. Chem.* **1988**, *9*, 101.
(36) James, A. D.; Murray, R. S. *J. Chem. Soc., Dalton Trans.* **1974**, 1273.
(37) Haim, A. *Comments Inorg. Chem.* **1985**, *4*, 113.

Two factors have been considered to be important in the stabilization of one or the other electronic isomer.[2] First, an electrostatic factor associated with the assembly of the mononuclear ions into the binuclear species. This was considered to be significant in favor of the higher stability of $[(NC)_5Fe^{II}(pz)Ru^{III}(NH_3)_5]$ by 0.09 V compared to its $[Fe^{III}(pz)Ru^{II}]$ isomer, because the electrostatics of the (+3, −3) combination is more favorable than the (+2, −2) one. Second, an "intrinsic" contribution, associated with the higher $E°$ in the $[Fe(CN)_5(pz)]^{2,3-}$ couple as compared to the $[Ru(NH_3)_5(pz)]^{3,2+}$ couple, which also favors the $[Fe^{II}(pz)Ru^{III}]$ state, by 0.03 V. In our CNpy system, a different picture arises; while the electrostatics favors the $[Fe^{II}(4pyCN)Ru^{III}]$ isomer by 0.04 V, the intrinsic component is now in favor of the $[Fe^{III}(4pyCN)Ru^{II}]$ distribution by 0.08 V (see Table 1). Summing up, the M_4 isomer, featuring $[Fe^{III}, Ru^{II}]$ states, should be favored over M'_4 by 0.04 V, a value similar to the one obtained through the thermodynamic cycle, 0.05 V. An additional example in which the intrinsic contribution highly overcomes the unfavorable electrostatic factor was shown for the $[(NH_3)_5Ru^{II}(pz)Ru^{III}(edta)]^+$ complex.[38]

By considering $K_{et4} = 0.13$, we obtain $k_{-3} = (8 \pm 3) \times 10^{-3}$ s^{-1}; this is significantly greater than the value found for the dissociation of 4-pyCN from $Fe^{II}(CN)_5(4pyCN)]^{3-}$, 1.02×10^{-3} s^{-1}.[12] The difference is consistent with the coordination of a MX_5^{3+} moiety to the remote nitrogen, decreasing the basicity of the adjacent nitrogen and hence weakening the Fe−N bond (as also found with the $[(NC)_5Fe^{II}(pyCN)Co^{III}(NH_3)_5]$ complex).[6]

A confirmation of the proposed dissociative decomposition mechanism is given by the results on the modified experiment with addition of $Mepz^+$ (Figure SI 3). In Figure SI 3a,b, the changes in the 350−550 nm range show also the $R_4 \rightarrow M_4$ process, followed by eqs 3−4, as in Figure SI 2. The new feature at 665 nm corresponds to eq 5:[21]

$$[Fe^{II}(CN)_5H_2O]^{3-} + Mepz^+ \rightarrow [Fe^{II}(CN)_5(Mepz)]^{2-} \qquad k_5 \tag{5}$$

It can be seen that $[Fe^{II}(CN)_5H_2O]^{3-}$ reacts competitively according to reactions 4 and 5. In Figure SI 3c the shift of the maximum at 425 nm toward lower wavelengths is indicative of the decay of $[Ru^{II}(NH_3)_5(4NCpy)]^{2+}$ and the appearance of $[Ru^{III}(NH_3)_5(4NHC(O)py)]^{2+}$, according to reactions 4(reverse) and 6.[3] Now, reaction 1(reverse) is not significant, because reaction 5 is faster.

$$[Ru^{III}(NH_3)_5(4NCpy)]^{3+} + H_2O \rightarrow [Ru^{III}(NH_3)_5(4NHC(O)py)]^{2+} + H^+ \qquad k_6 \tag{6}$$

Through reaction 6, we show the significance of hydrolytic reactions, associated with *mononuclear* $[Ru^{III}(NH_3)_5(4NCpy)]^{3+}$. We have no direct evidence of hydrolysis of M or M′. The dissociation and hydrolytic reactions of M'_4 are competitive processes, and the first reaction appears to be faster, leading to mononuclear products containing Fe(III) and Ru(II) species (eqs 3 and 4).[39] For longer times, Figure SI 2c,d showed that R_4 forms slowly, following the equilibration process of the mononuclear species in reaction 4. The concentration of $[Ru(NH_3)_5(4NCpy)]^{3+}$ grows at the same rate as R_4. As the Ru(III) mononuclear species is unstable toward hydrolysis (eq 6), reactions 3 and 4 are irreversibly driven. The spectral traces obtained in the experiment where $[Fe^{III}(CN)_5H_2O]^{2-}$ and $[Ru^{II}(NH_3)_5(4NCpy)]^{2+}$ are mixed (Figure SI 2d) were equal to those obtained in a simulation procedure, *only* if the hydrolysis of the mononuclear $[Ru(NH_3)_5(4NCpy)]^{3+}$ species (eq 6) was included in the simulation scheme; if not, the mononuclear species in reaction 4 and the R_4 complex equilibrate rapidly, with a minor amount of the latter species. Thus, the steady increase of the concentration of R_4 in the experiment is a consequence of the irreversibility originated in the hydrolytic reaction. The values of the rate constants for the hydrolysis reaction obtained through the kinetic analysis of a set of experiments are in the range $(1-5) \times 10^{-3}$ s^{-1}, in fair agreement with the value obtained by Yeh, 2.85×10^{-3} s^{-1}.[3]

From the E values for M_3, and through the onset of a thermodynamic cycle similar to the one displayed for M_4, we estimate $K_{et3} = 0.43$; i.e., about 30% of M'_3 could be present in the equilibrium mixture. For the dissociation reaction of the 3-CNpy-bridged mixed-valence complex, a scheme similar to that presented before (eqs 2−4) can be proposed. The k_{obs} value is higher than the one found for the 4-pyCN complex, and we obtain $k_d = (10 \pm 4) \times 10^{-3}$ s^{-1}; this is greater than the dissociation rate of the 4-CNpy bridged isomer, as expected.

The hydrolytic reactions of the 3-CNpy complexes display significantly lower rates compared to the 4-CNpy analogs.[3] Thus, Figure SI 4a shows the formation of M_3 and Figure SI 4b the dissociation and subsequent outer-sphere reaction leading to Fe(III) and Ru(II) species. In contrast to the results with M_4 (Figure SI 2c), the mononuclear products do not react in the longer time scale, because the hydrolysis of the $[Ru(NH_3)_5(3NCpy)]^{3+}$ ion is slow.

Finally, the possibility of disproportionation of the M complexes into the isovalent binuclear complexes should be considered. The equilibrium constant for the comproportionation reaction 7 was calculated from the appropriate redox potentials,[40] $K_c = 5.0 \times 10^2$

$$R_4^- + Ox_4^+ \leftrightarrow 2M_4 \qquad K_7 \tag{7}$$

As will be shown below, reaction 7 is part of the mechanistic scheme comprising the $R \rightarrow M \rightarrow Ox$ conversion in the reactions with peroxydisulfate (see Appendix, SI).

After correcting for the statistical factor, the stabilization of M_4 over the isovalent states in eq 7 is given by the free energy term $\Delta G_c = 1.4$ kcal mol^{-1} (0.06 V). As evidenced after consideration of the different factors which determine ΔG_c, the electronic delocalization contributes only slightly ($\alpha^2 = 0.03$ kcal mol^{-1}), as expected for a valence-trapped system. The electrostatic factor destabilizes the M_4 state, because electrostatic attractions in reactants and products are $2 \times 3 + 3 \times 2 = 12$ and $2 \times 2 \times 2 = 8$, respectively (a value lower than 0.5 kcal mol^{-1} is estimated from ion pair formation constants). Here, again, the species in the CNpy system behave similarly to the $[(NH_3)_5)Ru^{II}(pz)Ru^{III}(edta)]^+$ complex,[38] i.e., both mixed-valence species are electrostatically destabilized with respect to their isovalent states, in contrast with the results obtained with the $[(CN)_5Fe^{II}(pz)Ru^{III}(NH_3)_5]$ complex. In all of the three mixed-valence complexes the main stabilizing influence arises from the so-called "synergistic" factor associated with the M(II)−M(III) interaction. The loss of back-bonding upon oxidation of Ru(II)−L to Ru(III)−L is the dominant factor controlling the stability of M toward disproportionation.[38]

(iii) Ox Complexes. The changes in Figure SI 5a are similar as those seen in Figure SI 2a. In Figure SI 5b, the reaction with excess peroxydisulfate differs significantly from the one for the reaction with 1 equiv (Figure SI 2b). Although in both

(38) Ram, M. S.; Haim, A. *Inorg. Chem.* **1991**, *30*, 1319.

(39) k_h for M'_4 is assumed to be equal to the measured value for the $[(NC)_5Ru^{II}4pyCN\text{-}Ru^{III}(NH_3)_5]^+$ analog, $k_h = 1.5 \times 10^{-3}$ s^{-1} ($I = 0.1$ M, 25 °C).[32]

(40) Richardson, D. E.; Taube, H. *Coord. Chem. Rev.* **1984**, *60*, 107.

of them the decay of M_4 is observed, the products suggest the onset of reaction 8.[41]

$$[(NC)_5Fe^{III}(4pyCN)Ru^{II}(NH_3)_5] + S_2O_8^{2-} \rightarrow [(NC)_5Fe^{III}(4pyCN)Ru^{III}(NH_3)_5]^+ + SO_4^{2-} + SO_4^- \quad k_8 \quad (8)$$

In the time scale described by Figure SI 5b, the factor analysis suggests the presence of three species. As no spectral evidence of R_4 is detected, a new species must be forming. The latter is also in minor concentration compared to M_4 and Ox_4, and absorbs at ca. 390 nm. We propose that hydrolysis of Ox_4 is operative (eq 9).

$$[(NC)_5Fe^{III}(4pyCN)Ru^{III}(NH_3)_5]^+ + H_2O \rightarrow [NC)_5Fe^{III}(4pyC(O)NH)Ru^{III}(NH_3)_5] + H^+ \quad k_9 \quad (9)$$

In Figure SI 5c, the spectral changes are again associated with the appearance of a new species. This agrees with the complete factor analysis showing the onset of five colored species with a specific kinetic behavior. The long time scale is the least important for our present purposes, and it is probably related to decomposition processes following reactions 8 and 9.

Figure SI 6a shows mainly the $R_3 \rightarrow M_3$ conversion and Figure 6b the $M_3 \rightarrow Ox_3$ conversion. The factor analysis for both time-scales indicates that three species are absorbing. This confirms that no additional species associated with hydrolytic processes are disturbing, as was the case with the 4-CNpy isomers. Moreover, the fittings are very good without considering the hydrolysis reactions in the overall reaction scheme.

The higher reactivity of Ox *vs* M, M′ complexes toward hydrolysis is not unexpected; the positive charge at the N-bonded Ru(III) center is reinforced by the electron-withdrawing influence of the $[Fe^{III}(CN)_5^{2-}]$ moiety; interestingly, it has been found that the fully oxidized bis-pentaammineruthenium complex with bridging 4-CNpy hydrolyses with $k_h = 2.5 \times 10^{-2}$ s^{-1},[26] in agreement with the presently reported value for Ox_4 (Table 2). The value of k_h is smaller for the Ox_3 complex compared to Ox_4, as expected, and in agreement with the results for the corresponding mononuclear species. For the above mentioned reasons, the rates of hydrolysis of the Ox binuclear complexes are greater than the rates of similar processes for the mononuclear species.

Reactions of R and M with Peroxydisulfate: Kinetics and Mechanism. Scheme 1 resumes the main reactions considered to account for the spectral evolution observed. In the Appendix (SI) we describe in detail how we have performed the global analysis of the spectral changes observed in the reactions of R with peroxydisulfate. As a result of this analysis we have obtained the spectra of the individual species shown in Figure 1 and the values for the kinetic constants reported in Table 2. Using these parameters with the model in Scheme 1, the predicted and experimental kinetic traces are in excellent agreement, as shown in Figure 2 for the reaction of R_4 with peroxydisulfate.

We focus now on the nature of the reactive sites in the R and M species. The analysis must be consistent with the proposed structure for the mixed-valence complexes (both M_4 and M_3 with the corresponding electronic isomers), as well as with the characteristic rate constants previously obtained for other members of the $[(NC)_5Fe^{II}(L)Ru^{II}(NH_3)_5]^n$ series and other complexes in the reactions with peroxydisulfate.[2,29]

We propose that Ru is the oxidized center (eq 10), yielding the thermodynamically unstable electronic isomer, M′$_4$; this is based on kinetic considerations (all available data show that $[Ru^{II}(NH_3)_5^{2+}]$ centers react faster than $[Fe^{II}(CN)_5]^{3-}$ centers toward oxidation with peroxydisulfate).[9] The relative rates of the $[Ru(NH_3)_5(NCpy)]^{2+}$ and $[Fe(CN)_5(pyCN)]^{3-}$ ions with peroxydisulfate (Table 2) confirm this behavior. Thus, we rule out the alternative oxidation at the Fe(II) center.

$$[(NC)_5Fe^{II}(4pyCN)Ru^{II}(NH_3)_5]^- + S_2O_8^{2-} \rightarrow [(NC)_5Fe^{II}(4pyCN)Ru^{III}(NH_3)_5] + SO_4^{2-} + SO_4^- \quad k_{10} \quad (10)$$

A similar path was proposed for the first stage in the reaction of $[(NH_3)_5Ru^{II}(pz)Ru^{II}(edta)]$ with the same oxidant, i.e., oxidation at the $Ru^{II}(NH_3)_5^{2+}$ center, yielding also the unstable electronic isomer, $[(NH_3)_5Ru^{III}(pz)Ru^{II}(edta)]^+$. However, the latter complex evolved to the stable isomer, $[(NH_3)_5Ru^{II}(pz)$-$Ru^{III}(edta)]^+$, through a very rapid intramolecular electron-transfer process.[38] We are proposing the same for our system (eq 2), with the only difference that K_{et} is now appreciably greater compared to the value for the pz−binuclear complex, thus allowing for the existence of about 10% of M′$_4$ in the equilibrium (see above).

The value of k_{10} is smaller than corresponding values measured for the oxidation at the Ru(II) center in related complexes with pz and bpa as bridging ligands (bpa = 1,2-bis-(4-pyridyl)ethane).[2,29] A more quantitative interpretation of the *k* values for oxidation in different Ru(II) complexes will be given below.

After the very rapid intramolecular electronic isomerization process (eq 2), the M_4 complex, which is predominant to about 90% over M′$_4$, is able to react rapidly with peroxydisulfate, as far as a Ru(II) site is again available for oxidation; thus, the fully oxidized species, Ox_4, is obtained, according to eq 8.

The value of k_8 is smaller than k_{10} but is also consistent with oxidation at a Ru(II) center. The picture resembles again the reactivity of the $[(NH_3)_5Ru^{II}(pz)Ru^{III}(edta)]^+$ ion. The only difference stands on the omission of the comproportionation reaction in the latter system. This can be understood on the basis of a higher discrimination between both rate constants, i.e., the fully reduced complex appears to be completely transformed before the beginning of the reaction of the mixed-valence species with peroxydisulfate. In our system, however, the kinetic analysis shows that the Ox_4 species begins to be formed before the total consumption of R_4, thus allowing reaction 7 to proceed. The close values for k_{10} and k_8 agree with the above explanation. Reaction 7 involves an electron exchange between Ru and Fe metal centers; in fact, k_7 is comparable with the exchange rates in the related monomeric species, $[Ru(NH_3)_5(py)]^{2,3+}$ ($k_{ex} = 1.1 \times 10^5$ M^{-1} s^{-1}) and $[Fe(CN)_5(py)]^{2,3-}$ ($k_{ex} = 7 \times 10^5$ M^{-1} s^{-1}).[1]

In the above mentioned set of reactions, which we refer to as a [R → M′ ↔ M → Ox] scheme, the first stage yields the thermodynamically unstable but kinetically more accessible electronic isomer, M′. While M′ transforms rapidly to the dominant species, M, a new kinetically accessible site is open, Ru(II), and the reaction is completed. By comparison with the behavior of a related complex in the series, $[(NC)_5Fe(bpa)Ru$-$(NH_3)_5]^n$,[29] a reaction scheme which we call [R → M ↔ M′ → Ox] was proposed. Thus, R reacted in the first step yielding M, the kinetically accessible as well as the thermodynamically stable isomer $[Fe^{II}(bpa)Ru^{III}]$. The subsequent conversion to

(41) The sulfate radical generated in reaction 8 attacks another R species in a diffusion controlled process; cf.: Fürholz, U.; Haim, A. *Inorg. Chem.* **1987**, *26*, 3243.

Ox could be explained through the easy accessibility of M′ in the rapid equilibrium, making available the new Ru(II) site. A similar picture emerges for the oxidation of the pz-bridged complex in the same series. The first stage of the reaction (R → M) is also explained well on the above mentioned kinetic and thermodynamic considerations; the conversion to Ox could not be observed, however.[2]

The results for the 3-CNpy bridged dimer, R_3 (Table 2), show that a reaction scheme similar to that described for R_4 can be proposed. Thus, the corresponding values of k_8 and k_{10} are of the same order as that found for the 4-CNpy system, as expected from the close values of the redox potentials.

The reactions of the $[Ru^{II}(NH_3)_5L]$ species with peroxydisulfate provide an opportunity to test the Marcus relationship between k_{et} and $\Delta G°$ for a series of outer-sphere reactions that proceed in the intramolecular regime.[37] In a recent work,[42] we showed that the plot of ln k_{et}, the second-order rate constant for the oxidation with peroxydisulfate at different Ru(II) centers, against the electrode potential for the corresponding $Ru^{III,II}$ couples was linear, with a slope close to the theoretical value. In the plot, the presently reported values of k_8 and k_{10} were included, together with other rate constants for the Ru(II) oxidation at the $[X_5M(L)Ru^{II}(NH_3)_5]^n$ series. A wide range of rate constant values, k, and redox potential values, $E°_{Ru}$, were covered, including directly measured values for k or, alternatively, values derived on the basis of a mechanistic analysis as shown in the present work. Certainly, the fit of the plot adds further evidence to the complex reaction of Scheme 1. The inclusion of the cyanopyridine complexes adds a new feature to the overall picture of reactivity for different binuclear complexes with peroxydisulfate, namely, the presence of significant amounts of the two electronic isomers in the equilibrium mixtures, each one with its specific reactivity toward peroxydisulfate.

Acknowledgment. Our thanks go to the Consejo Nacional de Investigaciones Científicas y Técnicas (CONICET), the Universities of Buenos Aires and Mar del Plata, and the Deutsche Gesellschaft für Technische Zusammenarbeit Gmbh, for economic funding. J.A.O. is a member of the research staff of CONICET.

Supporting Information Available: Table containing calculated rate constants for the reaction of R_4 with excess peroxydisulfate, with different initial concentration of reactants (Table SI 1), Figures containing the cyclic voltammograms (Figure SI 1), the spectral changes in the reaction of R_4 with 1 equiv of oxidant (Figure SI 2), the same as before but with the initial addition of $Mepz^+$ (Figure SI 3), same as Figure SI 2 but for R_3 (Figure SI 4), spectral changes of R_4 with excess of oxidant (Figure SI 5), and same as before but for the R_3 isomer (Figure SI 6), text giving the Appendix describing the working details associated to the global analysis of some experiments (9 pages). Ordering information is given on any current masthead page.

IC960489Q

(42) Parise, A. M.; Baraldo, L. M.; Olabe, J. A. *Inorg. Chem.* **1996**, *35*, 5080.